Absolute Myocardial Blood Flow and Flow Reserve Assessed by Gated SPECT with Cadmium–Zinc–Telluride Detectors Using ^{99m}Tc-Tetrofosmin: Head-to-Head Comparison with ^{13}N-Ammonia PET

Rene Nkoulou*, Tobias A. Fuchs*, Aju P. Pazhenkottil, Silke M. Kuest, Jelena R. Ghadri, Julia Stehli, Michael Fiechter, Bernhard A. Herzog, Oliver Gaemperli, Ronny R. Buechel[†], and Philipp A. Kaufmann[†]

Department of Nuclear Medicine, Cardiac Imaging, University Hospital Zurich and University of Zurich, Zurich, Switzerland

Recent advances in SPECT technology including cadmium–zinc–telluride (CZT) semiconductor detector material may pave the way for absolute myocardial blood flow (MBF) measurements by SPECT. The aim of the present study was to compare K_1 uptake rate constants as surrogates of absolute MBF and myocardial flow reserve index (MFRi) in humans as assessed with a CZT SPECT camera versus PET. **Methods:** Absolute MBF was assessed in 28 consecutive patients undergoing adenosine stress–rest myocardial perfusion imaging (MPI) by ^{99m}Tc-tetrofosmin CZT SPECT and ^{13}N-ammonia PET, and MFR was calculated as a ratio of hyperemic over resting MBF. Results from both MPI methods were compared, and correlation coefficients were calculated. The diagnostic accuracy of CZT MFRi to predict an abnormal MFR defined as PET MFR less than 2 was assessed using a receiver-operator-characteristic curve. **Results:** Median MBF at rest was comparable between CZT and PET (0.89 [interquartile range (IQR), 0.77–1.00] vs. 0.92 [IQR, 0.78–1.06] mL/g/min; P = not significant) whereas it was significantly lower at stress in CZT than PET (1.11 [IQR, 1.00–1.26] vs. 2.06 [IQR, 1.48–2.56] mL/g/min; $P < 0.001$). This resulted in median MFRi values of 1.32 (IQR, 1.13–1.52) by CZT and 2.36 (IQR, 1.57–2.71) by PET ($P < 0.001$). The receiver-operator-characteristic curve revealed a cutoff for CZT MFRi at 1.26 to predict an abnormal PET MFR yielding an accuracy of 75%. **Conclusion:** The estimation of absolute MBF index values by CZT SPECT MPI with ^{99m}Tc-tetrofosmin is technically feasible, although hyperemic values are significantly lower than from PET with ^{13}N-ammonia, resulting in a substantial underestimation of MFR. Nevertheless, CZT MFRi may confer diagnostic value.

Key Words: myocardial flow reserve (MFR); myocardial blood flow (MBF); cadmium zinc telluride (CZT) SPECT; ^{13}N-ammonia PET

The definition of coronary artery disease (CAD) was originally based on the presence of anatomic luminal narrowing greater than 50%. Over the past decades, however, many advances in imaging techniques have enhanced our pathophysiologic understanding of CAD. It has been recognized that many factors beyond luminal narrowing may determine whether or not an anatomic coronary lesion induces ischemia. Because this cannot be comprehensively addressed by coronary angiography alone, nuclear myocardial perfusion imaging (MPI) has been well established as a tool for providing proof of ischemia. This is mandatory for prognostically relevant target lesion revascularization in chronic stable CAD. Because revascularization of a non–flow-limiting coronary stenosis is not beneficial to the patient, neither from a prognostic nor from a symptomatic point of view, nuclear MPI has been suggested as a gatekeeper for invasive coronary angiography (1–3). MPI studies with PET have demonstrated that absolute myocardial blood flow (MBF) and flow reserve (MFR) provide incremental diagnostic (4) and prognostic (5) information over relative perfusion alone. Quantitative assessment of MBF is difficult with standard SPECT for which detectors need to rotate around the patient and for which unfavorable properties of the currently available flow tracers hamper accurate MBF quantification because of nonlinear extraction fraction with roll-off at higher flow values. The recent advances in SPECT technology including semiconductor detector material (cadmium zinc telluride [CZT]) allow acquisition in a nonrotating mode and therefore acquisition of time–activity curves. This may enable absolute MBF and MFR estimation by SPECT as recently shown in experimental animal models (6), which may pave the way for its implementation in clinical routine (7). More knowledge on the impact of the tracer properties on the values obtained from quantification is crucial.

The aim of the present study was a head-to-head comparison in humans of indices of absolute MBF and MFR as assessed with ^{99m}Tc-tetrofosmin on a CZT SPECT camera versus MBF and MFR measured with ^{13}N-ammonia on a PET scanner.

MATERIALS AND METHODS

Patient Population

Thirty-two consecutive patients referred to nuclear MPI with either CZT SPECT or PET for clinical evaluation were enrolled. For study purposes, the patients underwent a second MPI with the respective other modality to obtain a pair of SPECT and PET myocardial
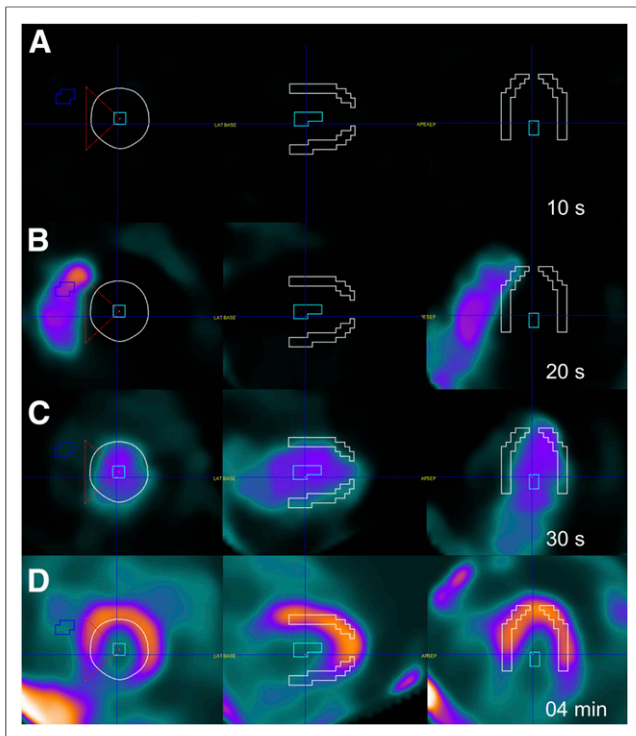
FIGURE 1. Dynamic CZT SPECT imaging during adenosine stress. (A) Short-axis (left) and vertical (middle) and horizontal long-axis (right) frames with regions of interest (ROIs) drawn in right and left ventricle and left ventricular myocardium. Dynamic acquisition sequentially illustrates right ventricular inflow (B), left ventricular inflow (C), and myocardial perfusion (D). White ROI = myocardium; light blue ROI = left ventricular cavity; dark blue ROI = right ventricular cavity; red triangle = delineation of upper and lower interventricular junction and middle of left ventricular cavity.

perfusion images for each patient. In patients without any therapeutic intervention (i.e., no revascularization and no change in medication) a time interval of 2 wk was accepted. In patients with no therapeutic intervention and chronic stable conditions, a maximal time interval of 12 wk was accepted. The sequence was SPECT first in 25 and PET first in 7 patients. The local ethics committee approved this study, and all subjects signed a written informed consent form.

[13]N-Ammonia PET

The PET MPI scan was acquired during pharmacologic stress with an adenosine protocol at a standard rate (0.14 mg/kg/min) over 6 min and at rest according to clinical standards (4,8). For the stress acquisition, ^{13}N-ammonia (1,053 ± 110 MBq) was injected 3 min into pharmacologic stress into a peripheral vein. Acquisition was repeated at rest (1,203 ± 148 MBq) 50 min after completion of the stress scan to allow for isotope decay. Images were acquired during 19 min in list-mode on a PET/CT scanner (Discovery ST/RX and Discovery VCT, both GE Healthcare). Images were reconstructed using a matrix of 128 × 128 and filtered backprojection into dynamic series encompassing the first 4 min (9 × 10, 6 × 15, and 3 × 20 s) for absolute MBF quantification and into a static series (15 remaining min) for assessment of relative perfusion abnormalities. A low-dose CT transmission scan was used for attenuation correction (9).
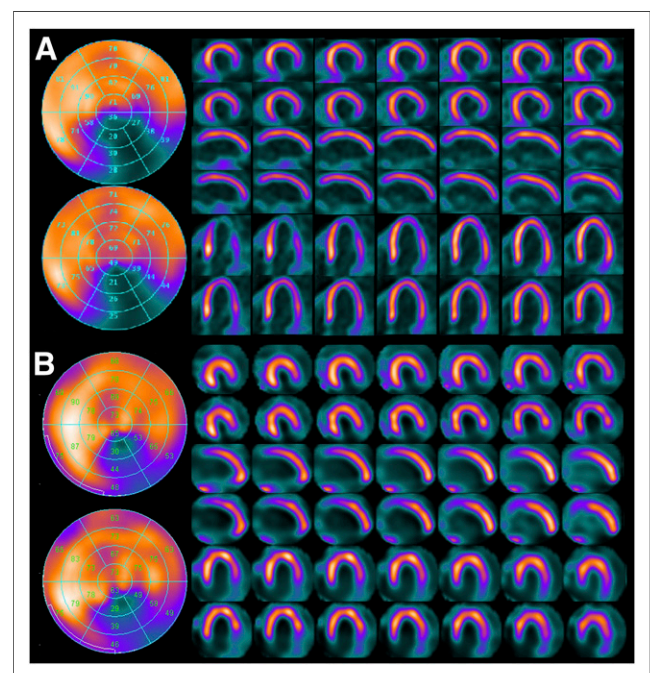
[99m]Tc-Tetrofosmin CZT SPECT

The CZT MPI scan was acquired on a hybrid SPECT/CT scanner (DNM 570c; GE Healthcare) using the 1-d stress–rest protocol identical

to the protocol described above. The SPECT part is a γ-camera with multipinhole collimation and 19 nonrotating pixelated CZT detector modules positioned around the patient's chest with full heart coverage (10). Due care was taken to ensure that patients were positioned in the middle of the field of view, and this was confirmed for each patient after the scan. A low-dose CT attenuation scan was acquired using the CT component of the same scanner (11). For the stress acquisition, ^{99m}Tc-tetrofosmin (330 ± 33 MBq) was injected 3 min into pharmacologic stress into a peripheral vein. Images were acquired in list-mode over 10 min starting immediately (a few seconds) before tracer injection. Five minutes after completion of the first scan, a second tracer injection with 3-fold-higher dose was administrated according to current guidelines, and the same acquisition protocol was applied (8). For logistic reasons, in 5 patients a rest–stress sequence was used for CZT scanning. Dynamic series including the first 4 min (6 × 10 and 6 × 30 s) were generated using a dedicated commercially available software package (Myovation for Alcyone; GE Healthcare) and reconstructed after attenuation correction using a maximum penalized likelihood iterative reconstruction (40 and 50 iterations applied for the stress and rest dataset, respectively) without scatter correction. A Butterworth postprocessing filter with cutoff frequency of 0.37 cycle/cm and order 7 was equally applied (10).

Absolute MBF Quantification

The MBF values for ^{13}N-ammonia PET (PET MBF) as well as the MBF index (MBFi) values for ^{99m}Tc-tetrofosmin CZT SPECT (CZT MBFi) were estimated using the commercially available PMOD software package (version 3.1; PMOD Technologies Ltd.) developed and validated at our institution (12,13). Regions of interest in the right ventricle cavity, left ventricle cavity, and covering the left ventricular myocardium were automatically generated and minimally modified as necessary by an experienced interpreter to best match cardiac anatomy and avoid contamination from extracardiac activity. A 1-tissue-compartment model

FIGURE 2. Static ^{99m}Tc-tetrofosmin CZT SPECT (A) and ^{13}N-ammonia PET (B) images acquired during stress (top) and at rest (bottom). Images were obtained from same patient as in Figure 1.

| Characteristic	n
Clinical symptoms	
Dyspnea	10 (35)
Typical chest pain	7 (25)
Atypical chest pain	9 (32)
Asymptomatic	6 (21)
Cardiovascular risk factors	
Smoking	4 (14)
Diabetes	9 (32)
Arterial hypertension	17 (61)
Dyslipidemia	18 (64)
Positive family history	13 (46)

Values are given as absolute numbers, with percentages in parentheses.

described by De Grado et al. was used for tracer kinetic modeling, inferring a myocardium tissue density of 1.04 g/mL (*14,15*). Global MBF values were determined after fitting the tissue activity curves of the myocardial as well as right ventricular and left ventricular values (*16*). No specific correction of the quantification process was performed despite the higher residual activity during the second half of the CZT study. Furthermore, no correction of the quantification model was applied despite differences in the extraction fraction and metabolites present for ^{99m}Tc-tetrofosmin compared with ammonia. Therefore, the MBF values obtained during the CZT study are rather indices of the flow (MBFi) at rest and stress, and their stress–rest ratio is the MFR index (MFRi). An image illustration during dynamic acquisition with CZT is displayed in Figure 1. For reasons of quality assurance, segments with CZT flow values greater than 4 mL/g/min or with more than 50% difference compared with adjacent segments were qualified as inconceivable values and were therefore discarded. This seemed appropriate to account for the tendency to greater contamination from extra cardiac activity and less favorable tracer distribution in addition to a lower spatial resolution of CZT than PET. Similarly, patients with global resting MBF PET values greater than 2 mL/min/g were excluded from further analysis because such values were classified as outliers (4 SDs above the reported mean values) according to a large body of evidence (*10*). Global MFR (PET) and MFRi (CZT) were calculated as the ratio of global MBF and MBFi at stress over rest values. Figure 2 depicts representative images of a patient's ^{99m}Tc-tetrofosmin CZT SPECT and ^{13}N-ammonia PET studies at stress and rest.

Statistical Analysis

The continuous values were summarized as mean $\pm$ SD and parametric values as percentage or median and interquartile range as appropriate. The Shapiro–Wilk test was used to test for normal distribution. Results from both MPI methods were compared using the Wilcoxon signed-rank test, and the Spearman correlation coefficient was calculated. A receiver-operator-characteristic analysis was conducted to evaluate the diagnostic accuracy of CZT in the detection of patients with MFR less than 2 by PET. All *P* values of less than 0.05 were considered statistically significant. SPSS 22.0 (SPSS) was used for the statistical analysis.
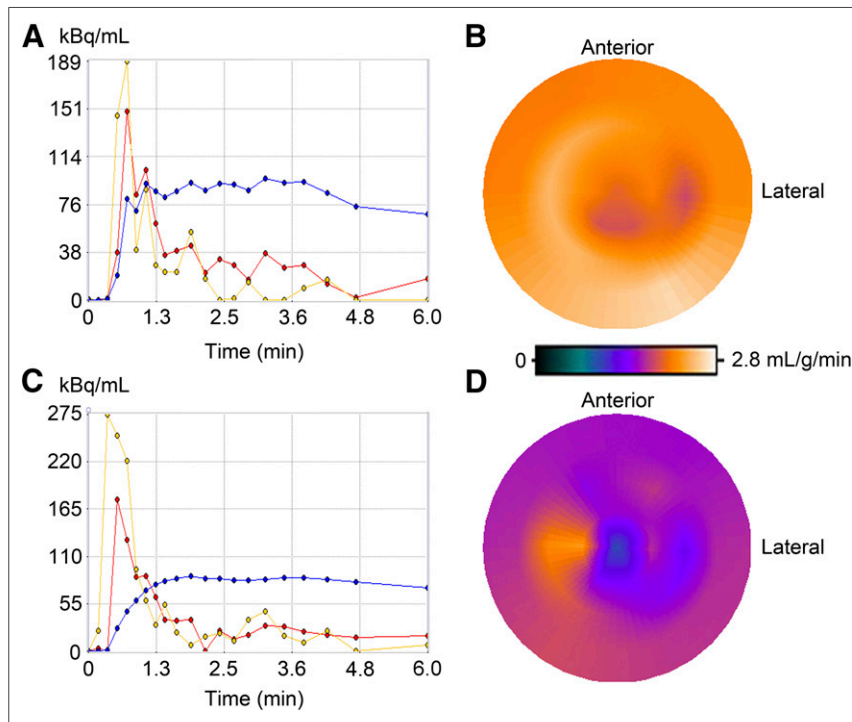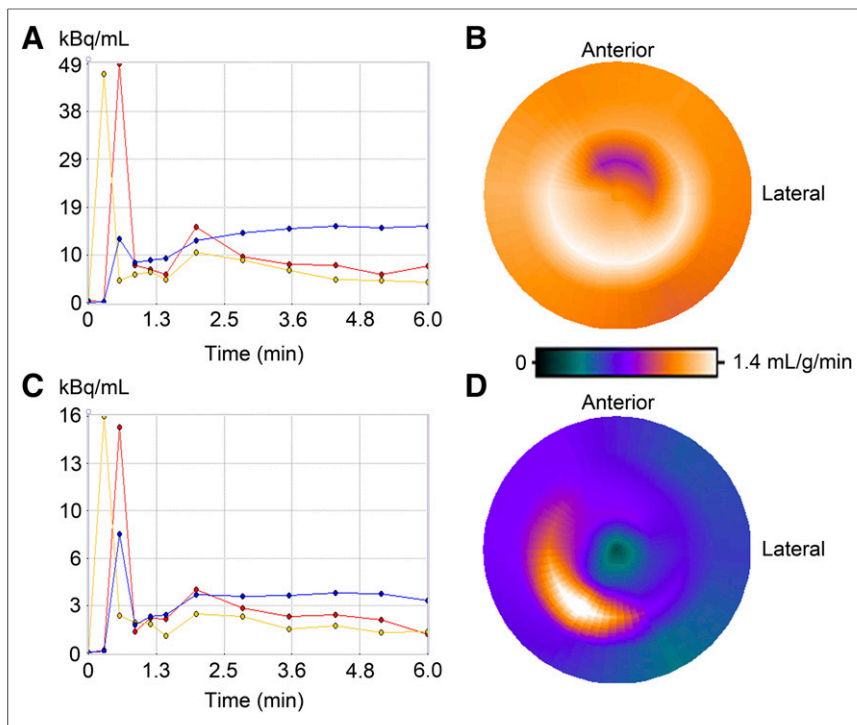

FIGURE 3. Fit curves and polar map of a representative patient when using PET: fit curves (A) and polar map (B) at stress and fit curves (C) and polar map (D) at rest. Yellow curves = right ventricle; red curves = left ventricle; blue curves = myocardium.

RESULTS

Four patients were excluded from further analysis according to predefined quality criteria for quantitative PET. The final study population consisted of 28 patients (86% men) with a mean age of 64 $\pm$ 10 y and a body mass index of 28 $\pm$ 6 kg/m^2 (Table 1). Kinetic modeling curves and polar maps at rest and stress for a representative patient are displayed using PET (Fig. 3) and CZT (Fig. 4).

A total of 952 segments (476 stress and 476 rest) were analyzed in the 28 patients by CZT and PET. According to prespecified quality criteria for CZT measurements, a total of 79 segments (8%) had to be excluded (28 stress and 51 rest scans). At rest, median MBFi with CZT was similar to MBF with PET (0.89 [interquartile range (IQR), 0.77–1.00] vs. 0.92 [IQR, 0.78–1.06] mL/g/min; *P* = not significant) whereas CZT MBFi was significantly lower at stress than PET MBF (1.11 [IQR, 1.00–1.26] vs. 2.06 [IQR, 1.48–2.56] mL/g/min; *P* < 0.001). This resulted in median MFRi values of 1.32 (IQR, 1.13–1.52) by CZT, which was significantly lower than the MFR value of 2.36 (IQR, 1.57–2.71) by PET (*P* < 0.001).

FIGURE 4. Fit curves and polar map of same patient as in Figure 3 when using CZT: fit curves (A) and polar map (B) at stress and fit curves (C) and polar map (D) at rest. Yellow curves = right ventricle; red curves = left ventricle; blue curves = myocardium.

Overall the correlation between CZT MBFi and PET MBF values was $\rho = 0.62$ ($P < 0.001$), whereas the correlations for MBFi and MBF at rest and stress were $\rho = 0.51$ ($P < 0.05$) and 0.30 (P = not significant) (Fig. 5).
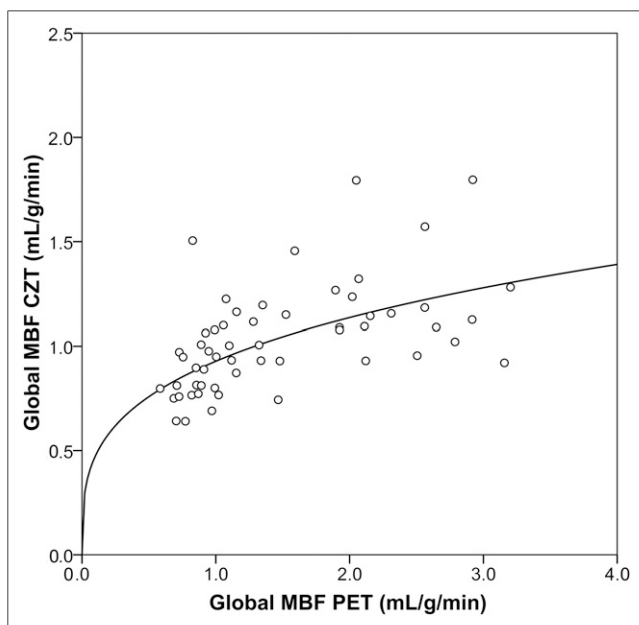
FIGURE 5. Head-to-head comparison of MBF values obtained from CZT SPECT versus PET, which served as standard of reference. Flattening of curve at values above 1 mL/g/min indicates underestimation by CZT SPECT particularly under high flow conditions.

The receiver-operator-characteristic curve revealed a cutoff for CZT MFRi at 1.26 to predict an abnormal PET MFR. When the latter cutoff value was used, CZT correctly identified 14 of 18 patients (specificity, 78%), with a PET MFR of 2 or greater, and 7 of 10 (sensitivity, 70%), with a PET MFR of less than 2, yielding an accuracy of 75% (Fig. 6). The MBF values at rest and stress in patients with correctly identified and misidentified PET MFR when using CZT is displayed in Table 2.

DISCUSSION

Our study is the first to compare in humans MBF data from dynamic CZT acquisition with data from PET, which is considered the gold standard for quantitative noninvasive MBF assessment (*17*). Our results demonstrate that quantification of dynamic SPECT MPI on modern CZT cameras is technically feasible but without specific correction for the different extraction fraction and metabolism of ^{99m}Tc-tetrofosmin underestimates MBF values at high flow conditions. Although resting MBFi values from CZT did not differ significantly from PET MBF values, hyperemic MBF values were significantly underestimated by CZT MBFi, resulting in underestimation of MFRi values obtained from CZT MBFi quantification. The key finding is that, nevertheless, values of CZT MFRi revealed an accuracy of 75% to assess an abnormal MFR documented by PET.

Previous studies exploring quantification of MBF with dynamic planar scintigraphy in humans (*18–25*) and with dynamic SPECT in experimental animals (*26–28*) have documented the limitations of conventional γ-cameras for the dynamic acquisition of datasets required for MBF quantification. The introduction of CZT cameras without the need of detector rotation has allowed proving the concept of dynamic image acquisition for MBF quantification in a recent animal study using microspheres as a standard of reference (*6*). A recent study has confirmed the feasibility and reproducibility of kinetic analysis of myocardial tracer uptake with a CZT device (*29*), although no standard of reference for perfusion quantification was available.

Our CZT MFRi values are in line with the values reported by Ben-Haim et al. (*29*) and are substantially lower than the MFR values estimated by PET. This was mainly driven by the lower MBF values observed by SPECT at high flow conditions, whereas resting MBF values were highly comparable with PET. This is explained at least in part by the well-known properties of ^{99m}Tc-tetrofosmin, namely inferior extraction at high flow rates compared with ^{13}N-ammonia. The superiority of ^{13}N-ammonia over ^{99m}Tc-tetrofosmin is not only evidenced by a higher extraction fraction at resting conditions (80% vs. 53%) but also based on the fact that the given extraction fraction remains constant over a much larger range of MBF. This explains why the model for correction of ^{13}N-ammonia MBF values may not
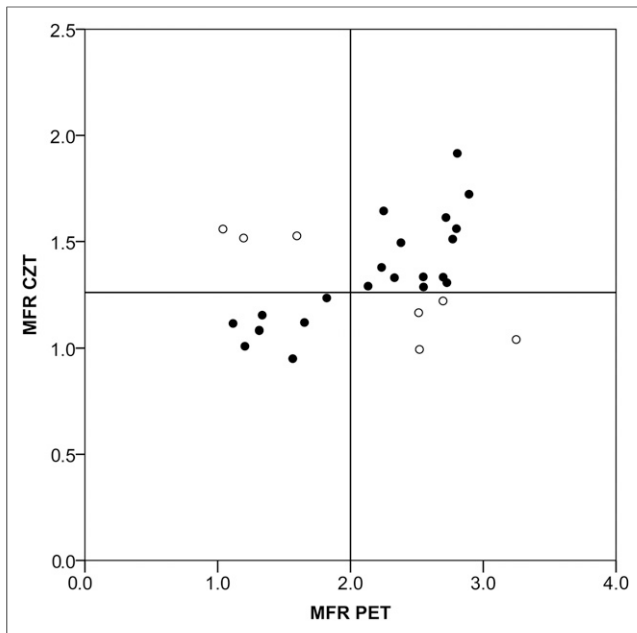
FIGURE 6. When cutoff value of 1.26 (as identified by receiver-operator-characteristic curve) was used for MFRi, CZT correctly identified (black circles) 14 of 18 patients (specificity, 78%) with PET MFR of 2 or greater and 7 of 10 patients (sensitivity, 70%) with PET MFR less than 2, resulting in accuracy of 75% for CZT MFRi.

provide a satisfying fit for ^{99m}Tc-tetrofosmin. Our results are in perfect agreement with the notion (6) that contrast between stress and resting flow will be lower for ^{99m}Tc tracers (23,29) than typically seen with PET (17).

However, in daily clinical practice qualitative SPECT MPI is a well-established tool for diagnostic and prognostic CAD estimation (30), indicating that despite the limited contrast of stress versus rest this technique provides powerful discrimination of health and disease in CAD. Given the growing body of evidence underlining the importance of absolute MBF and MFR quantification, our findings may have important clinical implications to further emphasize the role of SPECT MPI. In fact, although the MFR values were significantly lower by CZT than those assessed by PET due to the flattening of the curve at hyperemia, the CZT MFRi nevertheless confers a strong discriminatory power (accuracy of 75%) of normal versus abnormal myocardial perfusion. Despite the limited size of the study, the strength of these results lies in the fact that patients served as their own internal control and the

cutoff for abnormal perfusion detection was a PET MFR of less than 2, which is a robust and widely accepted threshold both for diagnostic (4) and prognostic CAD assessment (5,31). ^{99m}Tc-tetrofosmin was used in this study because it constitutes the most commonly used radiotracer for SPECT MPI in daily clinical routine. However, ^{99m}Tc tracers with more favorable tracer kinetics such as found for teboroxime (32) may help in improving the role of MFR by CZT.

It may be perceived as a potential limitation of the present study that no invasive coronary angiography was performed. However, the aim of the study was the evaluation of quantitative MBF and MFR assessed by CZT SPECT, and therefore quantitative PET perfusion seemed the most appropriate standard of reference while an anatomic definition of CAD could only provide dichotomous information on presence and absence of disease. Furthermore, an anatomic reference would represent a flawed gold standard for quantitative MBF measurements and would require assessment of invasive fractional flow reserve, which is not feasible for ethical reasons because of its invasive nature in patients with normal findings. Furthermore, we have confined our study to global rather than regional values, which may potentially constitute a limitation. However, global MFR reflects CAD beyond the epicardial section of the coronary tree involving microcirculation, including endothelial dysfunction, which has been shown to increase the sensitivity in detecting CAD when global MFR is used as an adjunct to PET MPI. The use of global MFR appears to be most appropriate when the aspect of microcirculatory dysfunction is included, which is often associated with CAD. Furthermore, for reasons of feasibility implementation of global MFR seems preferable over regional MFR because the reproducibility and the repeatability of global MFR are considerably superior to those of regional MFR from PET (13,33). This may apply even more for SPECT measurements because of technical issues and count statistics including lower spatial resolution, which may affect the apparent perfusion values in a nonhomogeneous manner, leading to different patterns in the polar plots for PET and SPECT as depicted in Figures 3 and 4. Differences are also based on biologic variability, because a profound spatial heterogeneity has been observed in regional MBF at rest and in response to vasodilator stress (34,35). The anatomic variability of the coronary trees is another source that has been shown to affect the per-segment performance of quantitative MBF measurements. Finally, our study has been performed using an integrated SPECT/CT but without scatter correction, and therefore extrapolation to protocols with separate acquisition on standalone CT and CZT SPECT scanners and to protocols using scatter correction should be done with caution.

TABLE 2
MBF Values at Rest and Stress in Patients with Correctly Identified and Misidentified PET MFRi When Using SPECT CZT

PET MFR	CZT MFRi	n	PET MBF stress	PET MBF rest	CZT MBFi stress	CZT MBFi rest
High	High	14	2.32 ± 0.45	0.91 ± 0.17	1.20 ± 0.23	0.87 ± 0.15
High	Low	4	2.39 ± 0.78	0.85 ± 0.22	1.14 ± 0.45	1.03 ± 0.32
Low	Low	7	1.57 ± 0.65	1.06 ± 0.27	1.04 ± 0.14	0.96 ± 0.17
Low	High	3	1.19 ± 0.43	0.90 ± 0.17	1.18 ± 0.17	0.82 ± 0.22

High PET MFR = myocardial flow rate $\geq$ 2 as assessed by PET (^{13}N-ammonia); low PET MFR = myocardial flow rate < 2 as assessed by PET; high CZT MFRi = myocardial flow rate $\geq$ 1.26 as assessed by SPECT CZT (^{99m}Tc-tetrofosmin); low CZT MFRi = myocardial flow rate < 1.26 as assessed by SPECT CZT. Values are mL/g/min ± SD.

CONCLUSION

Estimation of absolute MBFi values by CZT SPECT MPI with ^{99m}Tc-tetrofosmin is technically feasible, although hyperemic values are significantly lower than from PET with ^{13}N-ammonia, resulting in a substantial underestimation of MFR. Nevertheless, CZT MFRi may confer diagnostic value.

DISCLOSURE

ACKNOWLEDGMENTS

REFERENCES

1. Windecker S, Kolh P, Alfonso F, et al. 2014 ESC/EACTS guidelines on myocardial revascularization: the task force on myocardial revascularization of the European Society of Cardiology (ESC) and the European Association for Cardio-Thoracic Surgery (EACTS) developed with the special contribution of the European Association of Percutaneous Cardiovascular Interventions (EAPCI). *Eur Heart J.* 2014;35:2541–2619.

2. Herzog BA, Wyss CA, Husmann L, et al. First head-to-head comparison of effective radiation dose from low-dose 64-slice CT with prospective ECG-triggering versus invasive coronary angiography. *Heart.* 2009;95:1656–1661.

3. Hendel RC, Berman DS, Di Carli MF, et al. ACCF/ASNC/ACR/AHA/ASE/SCCT/SCMR/SNM 2009 appropriate use criteria for cardiac radionuclide imaging: a report of the American College of Cardiology Foundation Appropriate Use Criteria Task Force, the American Society of Nuclear Cardiology, the American College of Radiology, the American Heart Association, the American Society of Echocardiography, the Society of Cardiovascular Computed Tomography, the Society for Cardiovascular Magnetic Resonance, and the Society of Nuclear Medicine. *J Am Coll Cardiol.* 2009;53:2201–2229.

4. Ghadri JR, Fiechter M, Veraguth K, et al. Coronary calcium score as an adjunct to nuclear myocardial perfusion imaging for risk stratification before noncardiac surgery. *J Nucl Med.* 2012;53:1081–1086.

5. Herzog BA, Husmann L, Valenta I, et al. Long-term prognostic value of ^{13}N-ammonia myocardial perfusion positron emission tomography added value of coronary flow reserve. *J Am Coll Cardiol.* 2009;54:150–156.

6. Wells RG, Timmins R, Klein R, et al. Dynamic SPECT measurement of absolute myocardial blood flow in a porcine model. *J Nucl Med.* 2014;55:1685–1691.

7. Bocher M, Blevis IM, Tsukerman L, Shrem Y, Kovalski G, Volokh L. A fast cardiac gamma camera with dynamic SPECT capabilities: design, system validation and future potential. *Eur J Nucl Med Mol Imaging.* 2010;37:1887–1902.

8. Verberne HJ, Acampa W, Anagnostopoulos C, et al. EANM procedural guidelines for radionuclide myocardial perfusion imaging with SPECT and SPECT/CT: 2015 revision. *Eur J Nucl Med Mol Imaging.* 2015;42:1929–1940.

9. Koepfli P, Hany TF, Wyss CA, et al. CT attenuation correction for myocardial perfusion quantification using a PET/CT hybrid scanner. *J Nucl Med.* 2004;45:537–542.

10. Herzog BA, Buechel RR, Katz R, et al. Nuclear myocardial perfusion imaging with a cadmium-zinc-telluride detector technique: optimized protocol for scan time reduction. *J Nucl Med.* 2010;51:46–51.

11. Herzog BA, Buechel RR, Husmann L, et al. Validation of CT attenuation correction for high-speed myocardial perfusion imaging using a novel cadmium-zinc-telluride detector technique. *J Nucl Med.* 2010;51:1539–1544.

12. Siegrist PT, Gaemperli O, Koepfli P, et al. Repeatability of cold pressor test-induced flow increase assessed with H_2[15]O and PET. *J Nucl Med.* 2006;47:1420–1426.

13. Wyss CA, Koepfli P, Mikolajczyk K, Burger C, von Schulthess GK, Kaufmann PA. Bicycle exercise stress in PET for assessment of coronary flow reserve: repeatability and comparison with adenosine stress. *J Nucl Med.* 2003;44:146–154.

14. DeGrado TR, Hanson MW, Turkington TG, et al. Estimation of myocardial blood flow for longitudinal studies with ^{13}N-labeled ammonia and positron emission tomography. *J Nucl Cardiol.* 1996;3:494–507.

15. Nekolla SG, Reder S, Saraste A, et al. Evaluation of the novel myocardial perfusion positron-emission tomography tracer ^{18}F-BMS-747158-02: comparison to ^{13}N-ammonia and validation with microspheres in a pig model. *Circulation.* 2009;119:2333–2342.

16. Cerqueira MD, Weissman NJ, Dilsizian V, et al. Standardized myocardial segmentation and nomenclature for tomographic imaging of the heart: a statement for healthcare professionals from the Cardiac Imaging Committee of the Council on Clinical Cardiology of the American Heart Association. *Circulation.* 2002;105:539–542.

17. Gould KL, Johnson NP, Bateman TM, et al. Anatomic versus physiologic assessment of coronary artery disease: role of coronary flow reserve, fractional flow reserve, and positron emission tomography imaging in revascularization decision-making. *J Am Coll Cardiol.* 2013;62:1639–1653.

18. Taki J, Fujino S, Nakajima K, et al. ^{99m}Tc-sestamibi retention characteristics during pharmacologic hyperemia in human myocardium: comparison with coronary flow reserve measured by Doppler flowire. *J Nucl Med.* 2001;42:1457–1463.

19. Ito Y, Katoh C, Noriyasu K, et al. Estimation of myocardial blood flow and myocardial flow reserve by ^{99m}Tc-sestamibi imaging: comparison with the results of [^{15}O]H_2O PET. *Eur J Nucl Med Mol Imaging.* 2003;30:281–287.

20. Storto G, Cirillo P, Vicario ML, et al. Estimation of coronary flow reserve by Tc-99m sestamibi imaging in patients with coronary artery disease: comparison with the results of intracoronary Doppler technique. *J Nucl Cardiol.* 2004;11:682–688.

21. Storto G, Soricelli A, Pellegrino T, Petretta M, Cuocolo A. Assessment of the arterial input function for estimation of coronary flow reserve by single photon emission computed tomography: comparison of two different approaches. *Eur J Nucl Med Mol Imaging.* 2009;36:2034–2041.

22. Marini C, Giusti M, Armonino R, et al. Reduced coronary flow reserve in patients with primary hyperparathyroidism: a study by G-SPECT myocardial perfusion imaging. *Eur J Nucl Med Mol Imaging.* 2010;37:2256–2263.

23. Daniele S, Nappi C, Acampa W, et al. Incremental prognostic value of coronary flow reserve assessed with single-photon emission computed tomography. *J Nucl Cardiol.* 2011;18:612–619.

24. Alhassen F, Nguyen N, Bains S, et al. Myocardial blood flow measurement with a conventional dual-head SPECT/CT with spatiotemporal iterative reconstructions: a clinical feasibility study. *Am J Nucl Med Mol Imaging.* 2013;4:53–59.

25. Hsu B, Chen FC, Wu TC, et al. Quantitation of myocardial blood flow and myocardial flow reserve with ^{99m}Tc-sestamibi dynamic SPECT/CT to enhance detection of coronary artery disease. *Eur J Nucl Med Mol Imaging.* 2014;41:2294–2306.

26. Iida H, Eberl S. Quantitative assessment of regional myocardial blood flow with thallium-201 and SPECT. *J Nucl Cardiol.* 1998;5:313–331.

27. Christian TF, Peters K, Keck B, Allen J, Owens T, Borah B. Gated SPECT imaging to detect changes in myocardial blood flow during progressive coronary occlusion. *Int J Cardiovasc Imaging.* 2008;24:269–276.

28. Iida H, Eberl S, Kim KM, et al. Absolute quantitation of myocardial blood flow with (201)Tl and dynamic SPECT in canine: optimisation and validation of kinetic modelling. *Eur J Nucl Med Mol Imaging.* 2008;35:896–905.

29. Ben-Haim S, Murthy VL, Breault C, et al. Quantification of myocardial perfusion reserve using dynamic SPECT imaging in humans: a feasibility study. *J Nucl Med.* 2013;54:873–879.

30. Doukky R, Hayes K, Frogge N, et al. Impact of appropriate use on the prognostic value of single-photon emission computed tomography myocardial perfusion imaging. *Circulation.* 2013;128:1634–1643.

31. Ziadi MC, Dekemp RA, Williams KA, et al. Impaired myocardial flow reserve on rubidium-82 positron emission tomography imaging predicts adverse outcomes in patients assessed for myocardial ischemia. *J Am Coll Cardiol.* 2011;58:740–748.

32. Di Bella EV, Ross SG, Kadrmas DJ, et al. Compartmental modeling of technetium-99m-labeled teboroxime with dynamic single-photon emission computed tomography: comparison with static thallium-201 in a canine model. *Invest Radiol.* 2001;36:178–185.

33. Kaufmann PA, Gnecchi-Ruscone T, Yap JT, Rimoldi O, Camici PG. Assessment of the reproducibility of baseline and hyperemic myocardial blood flow measurements with ^{15}O-labeled water and PET. *J Nucl Med.* 1999;40:1848–1856.

34. Austin RE Jr, Aldea GS, Coggins DL, Flynn AE, Hoffman JI. Profound spatial heterogeneity of coronary reserve: discordance between patterns of resting and maximal myocardial blood flow. *Circ Res.* 1990;67:319–331.

35. Chareonthaitawee P, Kaufmann PA, Rimoldi O, Camici PG. Heterogeneity of resting and hyperemic myocardial blood flow in healthy humans. *Cardiovasc Res.* 2001;50:151–161.